Detection of negative ions in streamer discharge in air by transient cavity ringdown spectroscopy

Kimika Fushimi, Naoki Shirai, and Koichi Sasaki‡

Division of Applied Quantum Science and Engineering, Hokkaido University, Sapporo 060-8628, Japan

E-mail: sasaki@qe.eng.hokudai.ac.jp

Abstract. Atmospheric-pressure discharges generated in air are expected to be electronegative, but experiments that examine negative ion densities are limited to date. In this work, we measured the temporal variation of the negative ion density in a streamer discharge generated in air. We adopted cavity ringdown spectroscopy, where negative ions were detected via weak optical absorption caused by laser photodetachment. The temporal variation of the absolute negative ion density was deduced by the transient analysis of the ringdown curve. Negative ions were detected after the disappearance of the discharge voltage and current. The negative ion density started the increase at 0.4 μs after the initiation of the discharge. The increase means the enhancement of the electron attachment frequency in the late phase of the secondary streamer with electron cooling. The survival of electrons until 0.4 μs is understood by the steep decrease in the cross section of dissociative recombination with the electron energy. The maximum negative ion density was observed at 1 μs, and it was around the noise level at 1.5 μs. The rapid decay is consistent with the destruction of negative ions by mutual neutralization with positive ions.

Submitted to: *Plasma Sources Sci. Technol.*

Atmospheric-pressure nonequilibrium discharges have opened new applications of plasmas. Plasmas are frequently generated in ambient air in applications to medicine [1–3] and agriculture [4,5], since they should be in contact with targets which are not robust against vacuum (biological tissues, plant seeds, etc). Noble gases such as helium and argon are helpful to generate plasmas in ambient air [6, 7], but the plasmas are not pure noble gas discharges because of the unavoidable admixture of molecular species in air. The admixture of molecular species is indispensable in the applications, since they work as the sources of reactive radicals that promote plasma-induced chemistry.

It is noted here that oxygen and water vapor, which are major species in air, are electronegative. It is well known in low-pressure plasmas that electrons produced by ionization of neutral species react with electronegative molecules to form negative ions if

‡ Author to whom any correspondence should be addressed.

the plasmas are produced in electronegative gases [8, 9]. Considering the higher densities of oxygen and water vapor in atmospheric-pressure plasmas than conventional low-pressure plasmas, it is reasonable to expect that the dominant negative charges in atmospheric-pressure plasmas are not electrons but negative ions. In fact, many numerical simulations predict the domination of negative ions in atmospheric-pressure plasmas [10–13]. However, experimental investigations of negative ion densities in atmospheric-pressure plasmas are seriously limited to date.

A reason for the small number of experimental investigations on negative ions in atmospheric-pressure plasmas is the difficulty in the diagnostics. The negative ion densities in electronegative low-pressure plasmas are widely measured by probe-assisted laser photodetachment [14], but it is not applicable to atmospheric-pressure plasmas since Langmuir probes are ineffective. Experiments on negative ions in atmospheric-pressure plasmas mostly use mass spectrometers with sophisticated differential pumping systems [15–19]. However, the measurements are limited in the effluent regions since the transport of negative ions from the active discharge zone to a mass spectrometer is difficult. A recent work by Staps and coworkers succeeded in measuring the negative ion density in an atmospheric-pressure plasma jet by detecting the change in the refractive index of the plasma at the timing of laser photodetachment [20]. This method was originally used for measuring the negative ion density in a low-pressure plasma [21]. However, the derivation of the negative ion density is not straightforward in atmospheric-pressure plasmas since the refractive index is affected by both electron and gas densities. We recently reported the detection of negative ion species in an atmospheric-pressure dc discharge in ambient air by threshold photodetachment spectroscopy [22], but it was difficult to estimate the absolute densities of negative ions.

In this work, we determined the absolute density of negative ions in a streamer discharge generated in air on the basis of the optical absorption caused by laser photodetachment [23]. We needed the geometry of cavity ringdown spectroscopy (CRDS) [24, 25], since the optical absorption was weak because of the small cross section of photodetachment. The CRDS measurement may be problematic if the refractive index of the plasma is changed by the gas heating. For example, the detection of OH radicals in a slender burner flame by CRDS had difficulty in keeping the optical alignment of the cavity [26]. However, the streamer discharge with negligible gas heating was compatible with CRDS. A problem was the fact that the lifetime of the absorber was shorter than the ringdown time. We solved this issue by applying the transient analysis of the ringdown curve, and as a result, we succeeded in estimating the temporal variation of the absolute negative ion density.

The experimental setup is schematically shown in Fig. 1(a). The streamer discharge was generated between needle (the anode) and planar (the cathode) electrodes placed inside an optical cavity in air. The distance between the needle and planar electrodes was 7.5 mm, and the distance between the optical axis of the cavity and the needle electrode was 2.5 mm. The needle electrode was connected to a high-voltage pulsed power supply, and the planar electrode was electrically grounded. The duration of the high-voltage pulse was approximately 60 ns. The voltage between the needle and planar electrodes was measured using a high-voltage probe, while the current passing through the discharge was measured by

inserting a Rogowski coil between the planar electrode and the electrical ground. Figure 1(b) shows the optical emission image of the discharge, which was obtained by accumulating the images for 300 shots using a charge coupled device camera with a gated image intensifier. Slender streamers were observed in single-shot images. The spread image shown in Fig. 1(b) was observed in the accumulated measurement since the positions of the streamers fluctuated randomly from shot to shot.

The light source in the CRDS measurement was an optical parametric oscillator (OPO, MOPO HF made by Spectra-Physics) pumped by the third harmonics of an Nd:YAG laser. The wavelength and the duration of the OPO laser pulse were 777 nm (the idler output) and 10 ns, respectively, and the laser linewidth was approximately 0.1 cm^{-1} or 6 pm. The wavelength of 777 nm was the value indicated on the laser controller and its accuracy was approximately ± 0.1 nm. The linewidth of 0.1 cm^{-1} was the value indicated on the specification document. Thus, this is pulsed CRDS using a multimode laser, but single-mode cw CRDS is not necessary for detecting negative ions since the photodetachment cross section is constant within the linewidth of the pulsed laser. The timing of the laser oscillation was adjusted at 5 μs before the trigger of the high-voltage pulse. The repetition frequencies of the laser oscillation and the high-voltage pulse were 10 Hz. The OPO laser beam was injected into the optical cavity after passing through mode matching optics. The cavity mirrors with a high reflectivity at 770-785 nm had a radius of curvature of 2 m, and the cavity length was 20 cm. According to the theory of the optical cavity [27], the spot size of the laser field at the position of the discharge was estimated to be 0.3 mm. The laser pulse transmitted through the cavity was detected using a photomultiplier tube (PMT). An interference filter with the transmission at 780 ± 5 nm was placed in front of PMT to eliminate the signal output of the OPO laser at 653 nm and the optical emission of the discharge. The electrical signal from PMT, which showed the temporal variation of the transmitted laser intensity (the ringdown curve), was recorded using a digital oscilloscope. The waveforms of the pulsed high voltage and the discharge current were also recorded using the oscilloscope.

Typical ringdown curves are shown in Fig. 2. The vertical axis in Fig. 2 is plotted on a logarithmic scale. The ringdown curves were obtained by averaging 300 laser shots using the digital oscilloscope. Since the streamer discharges fluctuated from shot to shot, the ringdown curve for a single laser pulse was expected to be different for each laser pulse. However, we had to choose the average of 300 laser shots since the low-noise analysis of the single-shot ringdown curve was impossible. Therefore, the present experiment gave us the average negative ion density of 300 discharges. The signal-to-noise ratio was not improved by increasing the number of laser shots above 300. As shown in the figure, the ringdown curve in the absence of the discharge was approximated by an exponential function. When the discharge was ignited, we detected the superposition of the discharge noise at $0 \leq t \leq 0.3$ μs. After the noise disappeared ($0.4 \leq t \leq 1.5$ μs), we observed a steeper decrease in the transmitted laser intensity than that in the absence of the discharge. The slope of the semilogarithmic curve at $t \geq 1.5$ μs was almost the same as that in the absence of the discharge.

Conventional CRDS supposes a steady-state absorber, and the density of absorber is

deduced from the time constant of the exponential decrease in the transmitted laser intensity. However, it is apparent from Fig. 2 that the density of absorber has a faster temporal variation than the ringdown time constant. In this case, we can deduce the temporal variation of the absorber density by the transient analysis of the ringdown curve. The transmitted laser intensities in the absence and presence of the discharge are respectively governed by

$$\frac{\mathrm{d}I_0(t)}{\mathrm{d}t} = -\frac{1}{\tau_0} I_0(t) \tag{1}$$

and

$$\frac{\mathrm{d}I(t)}{\mathrm{d}t} = -\left(\frac{1}{\tau_0} + \frac{c}{L}\sigma n(t) l\right) I(t), \tag{2}$$

where $1/\tau_0 = c(1-R)/L$ is the ringdown frequency in the absence of the discharge with L, c, and R being the cavity length, the speed of light, and the reflectivity of the cavity mirrors, respectively, σ is the absorption cross section, $n(t)$ is the absorber density, and l is the length of the discharge zone along the axis of the cavity. $1/\tau_0 = 1.31 \times 10^5$ s^{-1} was evaluated from the ringdown curve shown in Fig. 2. We can deduce the absorber density by calculating

$$n(t) = -\frac{L}{c\sigma l}\left(\frac{1}{I(t)}\frac{\mathrm{d}I(t)}{\mathrm{d}t} + \frac{1}{\tau_0}\right). \tag{3}$$

We needed the moving average of the ringdown curve in the numerical calculation of $\mathrm{d}I(t)/\mathrm{d}t$, since the differential of the experimental ringdown curve was a noisy procedure. Figure 3 shows the temporal variation of the instantaneous ringdown frequency $-(\mathrm{d}I(t)/\mathrm{d}t)/I(t)$, which was obtained by applying the moving average for a duration of $\Delta t = 0.4$ μs to the waveform shown in Fig. 2. Similar calculations at shorter Δt suggest that the slightly higher ringdown frequency than that in the absence of the discharge ($1/\tau_0 = 1.31 \times 10^5$ s^{-1}) at $t \leq 0.3$ μs is caused by the discharge noise.

Since the photon energy at 777 nm exceeds the electron affinities of O^-, O_2^-, and H^- [28], the enhanced ringdown frequency observed at $0.4 \leq t \leq 1.5$ μs in Fig. 3 is considered to be caused by the disappearance of laser photons due to photodetachment of negative ions. Another possibility is optical absorption of neutral species: NO_2 [29], O_3 [30], O_2 (the A band, $b^1\Sigma_g^+ - X^3\Sigma_g^+$) [31], and N_2 (the first positive system, $B^3\Pi_g - A^3\Sigma_u^+$). However, the fast decay of the instantaneous ringdown frequency observed at $1 \leq t \leq 1.5$ μs is not consistent with absorption of NO_2, O_3, and O_2 since they are stable molecules at the electronic ground states. Although the variations in the vibrational and/or rotational temperatures would change the absorption strength even if the density is constant, it has been reported that the time constants of the vibrational and/or rotational temperatures in streamer discharges are much longer than 0.5 μs [32, 33]. In addition, it has been also reported that the decay of the $N_2(A^3\Sigma_u^+)$ density is also much slower than 0.5 μs [34, 35]. Therefore, it is difficult to suppose that NO_2, O_2, O_3, and $N_2(A^3\Sigma_u^+)$ are the absorbers for the enhanced ringdown frequency observed at $0.4 \leq t \leq 1.5$ μs, and the most likely species that cause the optical absorption with the short duration are negative ions. However, since we have not performed experiments with changing the laser wavelength, we cannot completely rule out the possibility that the optical absorption observed in this experiment is due to species other than negative ions.

We cannot show the data on the negative ion species in this paper, since we did not carry out the photodetachment experiment at multiple laser wavelengths. Considering the production kinetics, the most probable negative ion is O_2^-, which is produced by three-body electron attachment $O_2 + e + M \rightarrow O_2^- + M$. Since this reaction has the maximum rate coefficient at a low electron energy of 0.1 eV [36], the increase in the ringdown frequency at $t \geq 0.4$ μs, where the pulsed voltage between the electrodes is negligible, is consistent with the photodetachment of O_2^-. Since the cross section of dissociative recombination with positive ions decreases steeply with the electron energy [37], a high electron energy at an earlier delay time may allow electrons to survive without recombining with positive ions, resulting in the formation of O_2^- at $t \geq 0.4$ μs. In contrast, since the cross section of dissociative electron attachment to ground-state O_2 ($O_2 + e \rightarrow O^- + O$) has the threshold and the maximum at electron energies of 4.3 and 6.5 eV [38, 39], respectively, the production rate of O^- due to this reaction is expected to be low and the photodetachment of O^- is unlikely to participate in the enhanced ringdown frequency at $t \geq 0.4$ μs. However, some authors report the possibility of dissociative attachment of low-energy electrons to molecular oxygen at metastable and Rydberg states [40–42], and in addition, other authors report the domination of O^- in negative ion species in atmospheric-pressure plasmas [20, 22]. Furthermore, H^- is also produced by dissociative electron attachment to H_2O. Although we cannot determine the composition of negative ion species, in the following analysis, we try to estimate the absolute negative ion density by assuming O_2^- as the dominant negative ion species. Note that this is a tentative assumption, and we need further investigation to estimate the absolute negative ion density based on the knowledge on the composition of negative ion species.

The temporal variation of the negative ion density was obtained as shown in Fig. 4(a) by calculating Eq. (3), where we assumed $l = 3$ mm and $\sigma = 1 \times 10^{-22}$ m^2 [43], which is the photodetachment cross section of O_2^- at 777 nm. $l = 3$ mm was assumed by referring to the optical emission image shown in Fig. 1(b). The negative ion density started the increase at $t = 0.4$ μs, and the maximum negative ion density was observed at $t = 1$ μs. The maximum negative ion density was $\sim 2 \times 10^{20}$ m^{-3}, which is, to our best knowledge, the first measurement of the absolute negative ion density in atmospheric-pressure streamer discharge, even though it contains ambiguity due to the assumption of O_2^- as the dominant negative ion species. If the dominant negative ion species are O^- and H^-, the maximum density deduced from the same ringdown curve becomes 4×10^{19} and 5×10^{18} m^{-3}, respectively, since the photodetachment cross sections of O^- and H^- are 4.8×10^{-22} [44] and 4×10^{-21} m^2 [45] at 777 nm. Figures 4(b) and 4(c) show the waveforms of the pulsed voltage and the discharge current, respectively. It is understood from Fig. 4 that the increase in the negative ion density started after the disappearances of the discharge voltage and current. The decrease in the negative ion density was steep, and it was around the noise level at $t = 1.5$ μs.

It is well known that streamer discharge is composed of primary and secondary streamers [46]. The secondary streamer starts after the arrival of the primary streamer at the cathode. The speed of the primary streamer is dependent on the rise rate of the pulsed voltage, and in the case of 0.1 kV/ns in the present experiment, the expected arrival time of the primary streamer at the cathode is shorter than 50 ns [47]. Therefore, the temporal

resolution of the present experiment was insufficient to observe the phenomena in the primary streamer, and it is considered that Fig. 4(a) represents the evolution of the negative ion density in the secondary streamer.

According to a numerical simulation by Komuro and Ono, pairs of electrons and positive ions are predominantly produced in the primary streamer, and negative ions are minorities in the composition of negative charges [48]. The domination of electrons in negative charges is due to the fact that the reduced electric field is high in the primary streamer. The secondary streamer with a much lower reduced electric field enhances the electron attachment frequency to electronegative molecules, and as a result, the electron density becomes negligible in the late phase of the secondary streamer [48]. This process is the conversion from electrons to negative ions, and the plasma density does not charge so much in this period. Tomita and coworkers measured the electron density of 2.7×10^{20} m^{-3} in the initial phase of the secondary streamer by laser Thomson scattering [49]. The discharge was generated by applying a peak voltage of $\sim$ 25 kV between needle and planar electrodes with a distance of 13 mm. The maximum negative ion density shown in Fig. 4(a) is similar to the electron density measured by Tomita and coworkers [49]. Hence, the evolution of the absolute negative ion density shown in Fig. 4(a) is consistent with the assumption that almost all electrons produced in the primary streamer are lost due to attachment reactions to form negative ions in the late phase of the secondary streamer.

On the other hand, the decrease in the negative ion density at $1 \leq t \leq 1.5$ μs is consistent with the destruction of negative ions via mutual neutralization with positive ions. This is because the rate coefficient of mutual neutralization such as $O_2^- + O_2^+ \rightarrow O_2 + O_2$ is on the order of 10^{-13} m^3/s [50, 51]. A positive ion density of 10^{20} m^{-3} results in the destruction frequency of $> 10^6$ s^{-1} for negative ions, which can explain the lifetime of negative ions shown in Fig. 4(a). On the other hand, the rate coefficient of associative detachment $O_2^- + O \rightarrow O_3 + e$ is 2.5×10^{-16} m^3/s [52]. Hence, if the density of atomic oxygen is on the order of 10^{22} m^{-3}, which is possible in streamer discharges [53], the destruction frequency of negative ions can be $> 10^6$ s^{-1}. However, since electrons produced via associative detachment may be lost due to attachment reactions to form negative ions again, resulting in a quasi-stationary negative ion density after the maximum. Therefore, the steep decay of the negative ion density at $1 \leq t \leq 1.5$ μs is not explained by associative detachment, and it is likely that mutual neutralization with positive ions is the dominant destruction process of negative ions.

In summary, we have demonstrated the measurement of the absolute negative ion density in a streamer discharge in air by transient CRDS. Considering the delay time for the appearance and the absolute negative ion density, the production of the negative ions is owing to electron attachment processes to electronegative molecules in the late phase of the secondary streamer. The decay time constant of the negative ion density is consistent with the destruction due to mutual neutralization. The present work shows the applicability of transient CRDS to the measurement of negative ion densities in atmospheric-pressure discharges.

Acknowledgments

The authors are grateful to Uwe Czarnetzki for his advice on the transient analysis of the ringdown curve.

References

[1] Fridman G, Friedman G, Gutsol A, Shekhter A B, Vasilets V N and Fridman A 2008 Plasma Process. Polym. **5** 503
[2] Kong M G, Kroesen G, Morfill G, Nosenko T, Shimizu T, van Dijk J and Zimmermann J L 2009 New J. Phys. **11** 115012
[3] Weltmann K-D and von Woedtke T 2017 Plasma Phys. Control. Fusion **59** 014031
[4] Puač N, Gherardi M and Shiratani M 2018 Plasma Process. Polym. **15** e1700174
[5] Ranieri P, Sponsel N, Kizer J, Rojas-Pierce M, Hernández R, Gatiboni L, Grunden A and Stapelmann K 2021 Plasma Process. Polym. **18** e2000162
[6] Bekeschus S, Schmidt A, Weltmann K-D and von Woedtke T 2016 Clin. Plasma Med. **4** 19
[7] Golda J, Held J, Redeker B, Konkowski M, Beijer P, Sobota A, Kroesen G, Braithwaite N St J, Reuter S, Turner M M, Gans T, O'Connell D and Schulz-von der Gathen V 2016 J. Phys. D: Appl. Phys. **49** 084003
[8] Wong A Y, Mamas D L and Arnush D 1975 Phys. Fluids **18** 1489
[9] Ahn T H, Nakamura K and Sugai H 1996 Plasma Sources Sci. Technol. **5** 139
[10] Liu D-X, Rong M-Z, Wang X-H, Iza F, Kong M G and Bruggeman P 2010 Plasma Process. Polym. **7** 846
[11] Hemke T, Wollny A, Gebhardt M, Brinkmann R P and Mussenbrock T 2011 J. Phys. D: Appl. Phys. **44** 285206
[12] Kelly S and Turner M M 2014 Plasma Sources Sci. Technol. **23** 065013
[13] Lietz A M and Kushner M J 2016 J. Phys. D: Appl. Phys. **49** 425204
[14] Bacal M, Hamilton G W, Bruneteau A M and Doucet J 1979 Rev. Sci. Instrum. **50** 719
[15] Bruggeman P, Iza F, Lauwers D and Gonzalvo Y A 2010 J. Phys. D: Appl. Phys. **43** 012003
[16] Oh J-S, Gonzalvo Y A and Bradley J W 2011 J. Phys. D: Appl. Phys. **44** 365202
[17] McKay K, Walsh J L and Bradley J W 2013 Plasma Sources Sci. Technol. **22** 035005
[18] Groβe-Kreul S, Hübner S, Schneider S, Ellerweg D, von Keudell A, Matejčík S and Benedikt J 2015 Plasma Sources Sci. Technol. **24** 044008
[19] Chen B and Liu D 2021 IEEE Trans. Plasma Sci. **49** 1190
[20] Staps T J A, Donders T J M, Platier B and Beckers J 2022 Plasma Sources Sci. Technol. **31** 025010
[21] Haverlag M, Kono A, Passchier D, Kroesen G M W, Goedheer W J and de Hoog F J 1991 J. Appl. Phys. **70** 3472
[22] Sasaki K, Hosoda R and Shirai N 2020 Plasma Sources Sci. Technol. **29** 085012
[23] Quandt E, Döbele H F and Graham W G 1998 Appl. Phys. Lett. **72** 2394
[24] Quandt E, Kraemer I and Döbele H F 1999 Europhys. Lett. **45** 32
[25] Booth J P, Corr C S, Curley G A, Jolly J and Guillon J 2006 Appl. Phys. Lett. **88**, 151502
[26] Zaima K, Tomioka S and Sasaki K 2015 Jpn. J. Appl. Phys. **54** 088005
[27] Yariv A 1991 *Optical Electronics, 4th ed.*, Saunders College Publishing, Philadelphia USA, Chap. 4.
[28] Rienstra-Kiracofe J C, Tschumper G S and Schaefer III H F 2002 Chem. Rev. **102** 231
[29] Kirmse B, Delon A and Jost R 1997 J. Geophys. Res. **102** 16089
[30] Gorshelev V, Serdyuchenko A, Weber M, Chehade W and Burrows J P 2014 Atmos. Meas. Tech. **7** 609
[31] Brown L R and Plymate C 2000 J. Mol. Spectrosc. **199** 166
[32] Pendleton J, Montello A, Carter C, Lempert W and Gundersen M A 2012 J. Phys. D: Appl. Phys. **45** 495401
[33] Ono R 2018 J. Phys. D: Appl. Phys. **51** 245202
[34] Šimek M 2003 Plasma Sources Sci. Technol. **12** 454
[35] Ono R, Tobaru C, Teramoto Y and Oda T 2009 Plasma Sources Sci. Technol. **18** 025006

[36] Chanin L M, Phelps A V and Biondi M A 1962 Phys. Rev. **128** 219
[37] Peterson J R, Le Padellec A, Danared H, Dunn G H, Larsson M, Larson A, Peverall R, Strömholm C, Rosén S, af Ugglas M and van der Zande W J 1998 J. Chem. Phys. **108** 1978
[38] Henderson W R, Fite W L and Brackmann R T 1969 Phys. Rev. **183** 157
[39] Itikawa Y 2009 J. Phys. Chem. Ref. Data **38** 1
[40] Hayashi D and Kadota K 1999 Jpn. J. Appl. Phys. **37** 225
[41] Katsch H M, Sturm T, Quandt E and Döbele H F 2000 Plasma Sources Sci. Technol. **9** 323
[42] Ding W X, Pinnaduwage L A, Tav C and McCorkle D L 1999 Plasma Sources Sci. Technol. **8** 384
[43] Lee L C and Smith G P 1979 J. Chem. Phys. **70** 1727
[44] Génévriez M, Dunseath K M, Terao-Dunseath M, Hibbert A, Dochain A, Marion R and Urbain X 2018 Phys. Rev. A **98** 033410
[45] Smith S J and Burch D S 1959 Phys. Rev. Lett. **2** 165
[46] Tochikubo F and Komuro A 2021 Jpn. J. Appl. Phys. **60** 040501
[47] Komuro A, Ryu T, Yoshino A, Namihira T, Wang D and Ono R 2021 J. Phys. D: Appl. Phys. **54** 364004
[48] Komuro A and Ono R 2014 IEEE Trans. Plasma Sci. **42** 2406
[49] Tomita K, Inada Y, Komuro A, Zhang X, Uchino K and Ono R 2020 J. Phys. D: Appl. Phys. **53** 08LT01
[50] Peterson J R, Aberth W H, Moseley J T and Sheridan J R 1971 Phys. Rev. A **3** 1651
[51] Moseley J T, Aberth W and Peterson J R 1972 J. Geophys. Res. **77** 255
[52] Ferguson E E 1967 Rev. Geophys. **5** 305
[53] Pendleton S J, Bowman S, Carter C, Gundersen M A and Lempert W 2013 J. Phys. D: Appl. Phys. **46** 305202

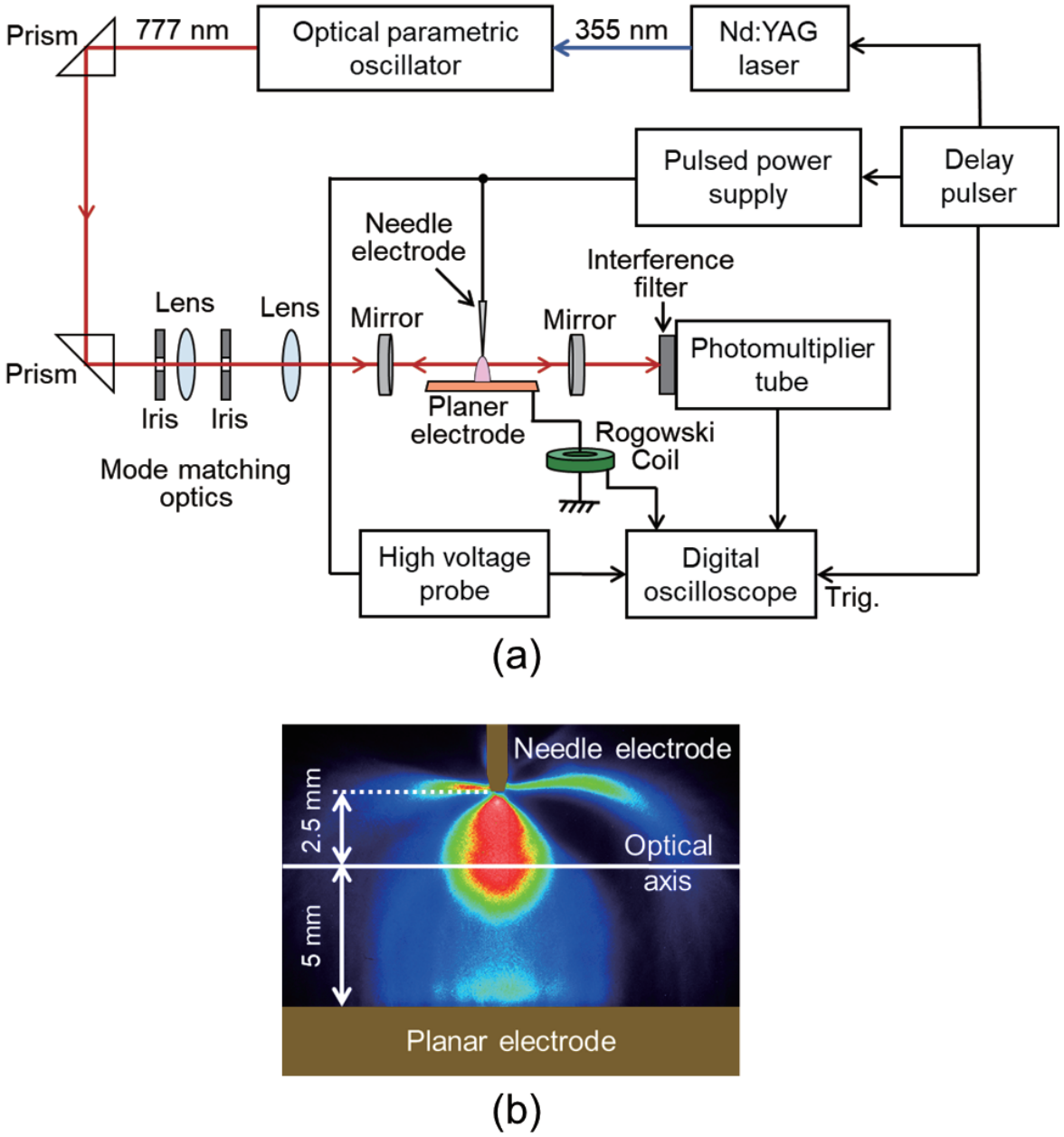

Figure 1. (a) Block diagram of experimental setup. (b) Optical emission image of streamer discharge together with positions of electrodes and optical axis.

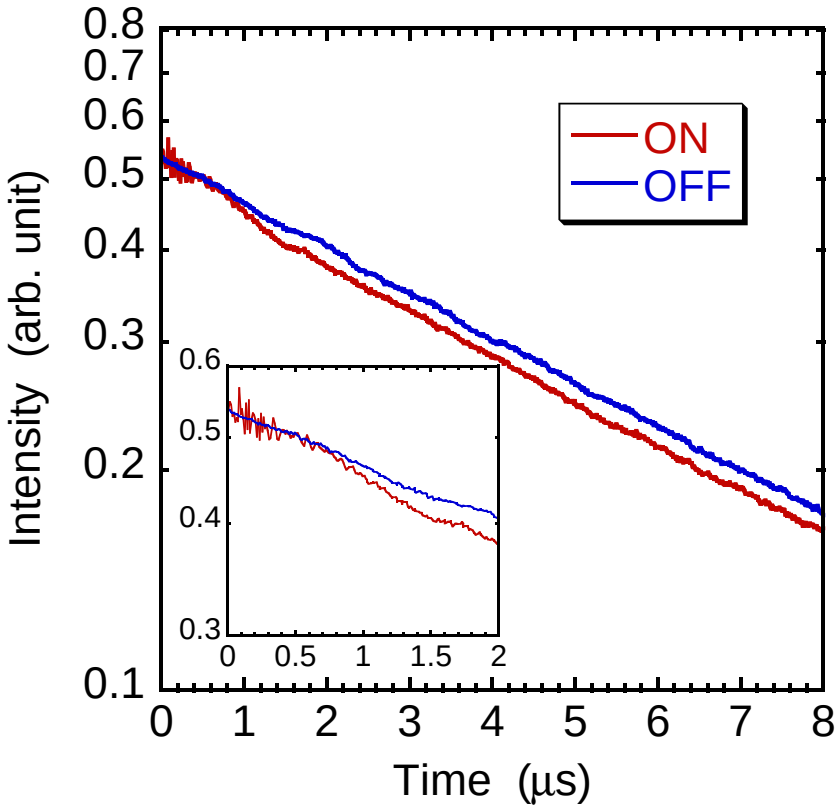

Figure 2. Typical ringdown curves observed in the presence and absence of streamer discharge. The vertical axis is plotted on a logarithmic scale. The inset shows the expanded view of the important part.

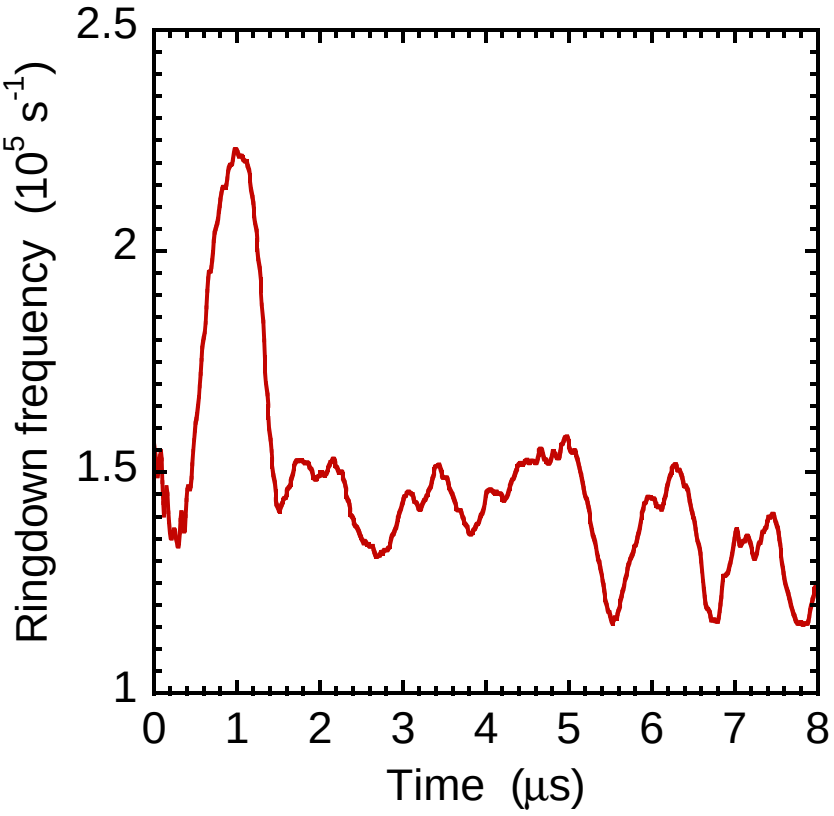

Figure 3. Temporal variation of instantaneous ringdown frequency obtained from ringdown curve observed in presence of streamer discharge. The instantaneous ringdown frequency was obtained by calculating $-(\mathrm{d}I(t)/\mathrm{d}t)/I(t)$, where $I(t)$ represents the temporal variation of the transmitted laser intensity.

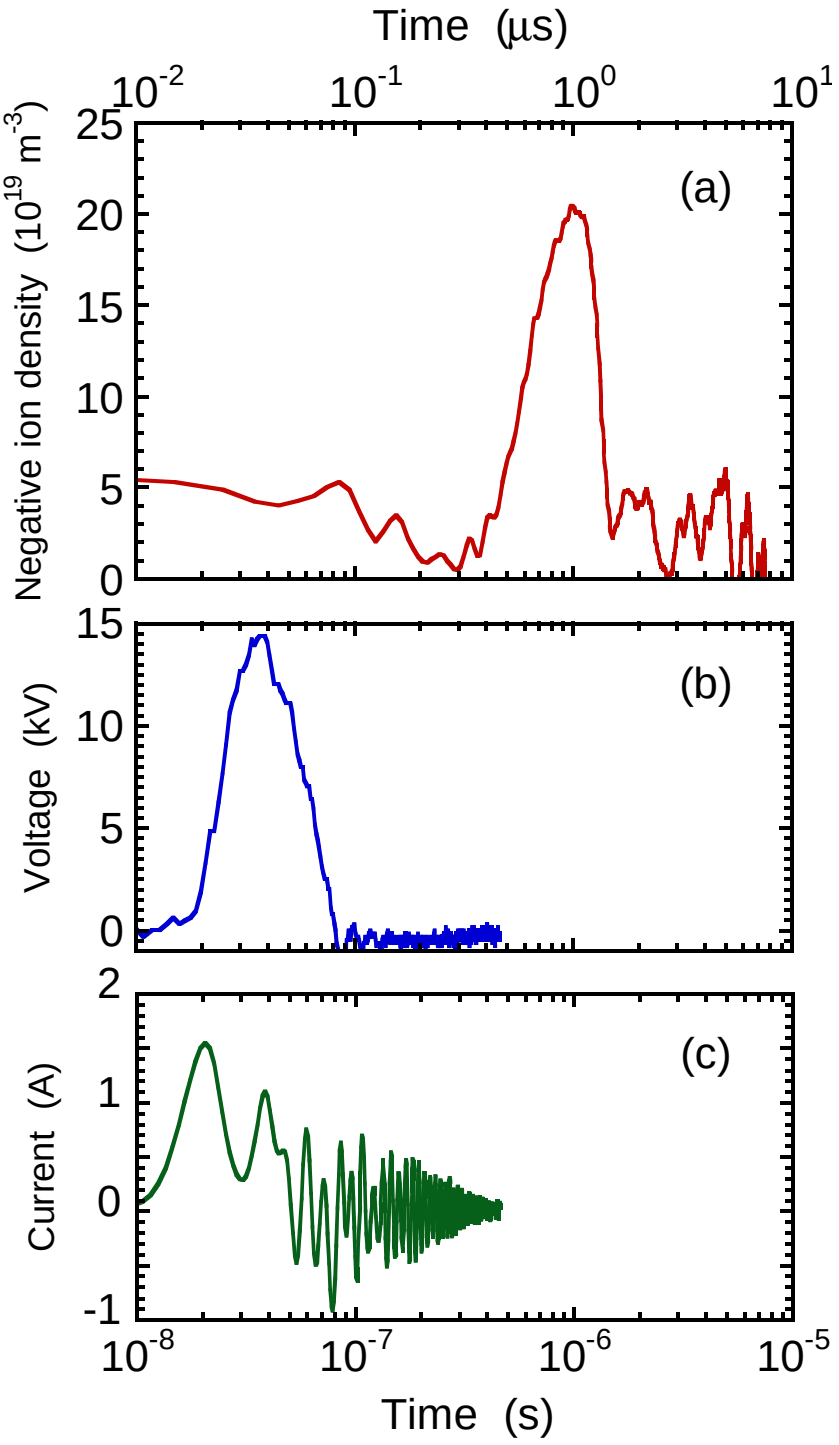

Figure 4. Temporal variations of (a) negative ion density, (b) discharge voltage, and (c) discharge current.